(2)

SRI International

AD-A261 099

DTIC
S ELECTE D
FEB 2 3 1993
C

Quarterly Technical Report 2 • February 1993

IR MATERIALS PRODUCIBILITY

A. Sher, Program Director
M.A. Berding, Sr. Research Physicist
A.T. Paxton, Research Physicist
Physical Electronics Laboratory

M.W. Muller, Consultant

SRI Project 3820

Prepared for:

Contracting Officers Technical Representative
Defense Advanced Research Projects Agency
Microelectronics Technology Office (MTO)
3701 N. Fairfax Drive
Arlington, VA 22203-1714

Attn: Mr. Raymond Balcerak

93-03608

ARPA Order No. 8557; Program Code Nos. 2H20, 2D10

Contract MDA972-92-C-0053

Covering the period: 1 November 1992 through 31 January 1993

The views and conclusions contained in this document are those of the authors and should not be interpreted as representing the official policies, either expressed or implied, of the Defense Advanced Research Projects Agency or the U.S. Government.

Approved for Public Release
Distribution Unlimited

Quarterly Technical Report 2 • February 1993

IR MATERIALS PRODUCIBILITY

A. Sher, Program Director
M.A. Berding, Sr. Research Physicist
A.T. Paxton, Research Physicist
Physical Electronics Laboratory

M.W. Muller, Consultant

SRI Project 3820

Accesion For		
NTIS CRA&I	☑	
DTIC TAB	☐	
Unannounced	☐	
Justification		
By		
Distribution /		
Availability Codes		
Dist	Avail and / or Special	
A-1		

DTIC QUALITY INSPECTED 3

Prepared for:

Contracting Officers Technical Representative
Defense Advanced Research Projects Agency
Microelectronics Technology Office (MTO)
3701 N. Fairfax Drive
Arlington, VA 22203-1714

Attn: Mr. Raymond Balcerak

Sponsored by:

Defense Advanced Research Projects Agency
Microelectronics Technology Office (MTO)
Infrared Focal Plane Array Program
ARPA Order No. 8557; Program Code Nos. 2H20, 2D10
Issued by DARPA/CMO under Contract MDA972-92-C-0053

Covering the period: 1 November 1992 through 31 January 1993

The views and conclusions contained in this document are those of the authors and should not be interpreted as representing the official policies, either expressed or implied, of the Defense Advanced Research Projects Agency or the U.S. Government.

Approved for Public Release
Distribution Unlimited

Approved:

Ivor Brodie, Director
Physical Electronics Laboratory
Computing and Engineering Sciences Division

SRI International 333 Ravenswood Avenue • Menlo Park, CA 94025-3493 • (415) 326-6200 • FAX (415) 326-5512 • Telex 334486

REPORT DOCUMENTATION PAGE

Form Approved OMB No. 0704-0188

Public reporting burden for this collection of information is estimated to average 1 hour per response, including the time for reviewing instructions, searching existing data sources, gathering and maintaining the data needed, and completing and reviewing the collection of information. Send comments regarding this burden estimate or any other aspect of this collection of information, including suggestions for reducing this burden, to Washington Headquarters Services, Directorate for Information Operations and Reports, 1215 Jefferson Davis Highway, Suite 1204, Arlington, VA 22202-4302, and to the Office of Management and Budget, Paperwork Reduction Project (0704-0188), Washington, DC 20503.

1. AGENCY USE ONLY *(Leave Blank)*

2. REPORT DATE
February 1993

3. REPORT TYPE AND DATES COVERED
Quarterly Tech. Rpt. 2, 11-1-92 to 1-31-93

4. TITLE AND SUBTITLE
IR Materials Producibility

5. FUNDING NUMBERS

6. AUTHOR(S)
A. Sher, M.A. Berding, A.T. Paxton, SRI International
M. Muller, Consultant

7. PERFORMING ORGANIZATION NAME(S) AND ADDRESS(ES)
SRI International
333 Ravenswood Avenue
Menlo Park, CA 94025

8. PERFORMING ORGANIZATION REPORT NUMBER

9. SPONSORING/MONITORING AGENCY NAME(S) AND ADDRESS(ES)
Defense Advanced Research Projects Agency
Microelectronics Technology Office (MTO)
Infrared Focal Plane Array Program
3701 N. Fairfax Drive
Arlington, VA 22203-1714

10. SPONSORING/MONITORING AGENCY REPORT NUMBER

11. SUPPLEMENTARY NOTES

12a. DISTRIBUTION/AVAILABILITY STATEMENT
Approved for public release; distribution unlimited

12b. DISTRIBUTION CODE

13. ABSTRACT *(Maximum 200 words)*

We have begun the calculation of relaxation of the near neighbors about the native defects in HgCdTe. We have found that approximate self-consistent schemes are inadequate for the large displacements of the highly strained defects, and therefore these calculations are being done self-consistently. The fields produced by long-range strain fields of dislocations via the piezoelectric effect and charged dislocation cores have been calculated for HgCdTe. The impact of dislocation core charges depends on the location of the dislocation and is greater in the depletion region where the screening is reduced, and smaller in the neutral regions of the device. We also find that their impact decreases as the temperature is increased. We have completed the calculations of the unrelaxed native point defect energies in ZnSe within the local density approximation and have begun the calculation of the gradient correction to these energies. Based on these preliminary numbers, we predict the zinc vacancy and the zinc antisite, and the zinc interstitial to be the dominant defects in ZnSe. We are currently calculating the relaxation about the most important defects in ZnSe.

14. SUBJECT TERMS
native point defect; defect density; photonic material; IRFPA; dislocation; HgTe; CdTe; ZnSe; HgCdTe

15. NUMBER OF PAGES
19

16. PRICE CODE

17. SECURITY CLASSIFICATION OF REPORT	18. SECURITY CLASSIFICATION OF THIS PAGE	19. SECURITY CLASSIFICATION OF ABSTRACT	20. LIMITATION OF ABSTRACT
Unclassified	Unclassified	Unclassified	None

SUMMARY

We have begun the calculation of relaxation about the native point defect in HgCdTe. We have found that approximate self-consistent schemes are inadequate for the large displacements of the highly strained defects; therefore, these calculations are being done self-consistently, and thus are computationally time-consuming. The fields produced by long-range strain fields of dislocations via the piezoelectric effect and charged dislocation cores have been calculated. We find that the piezoelectric potential is a superposition of cylindrical quadrupole and hexadecapole terms. The impact of dislocation core charges depends on the location of the dislocation, and is greater in the depletion region where the screening is reduced, and smaller in the neutral regions of the device. We also find that the impact decreases as the temperature is increased. We have completed the calculations of the unrelaxed native point defect energies in ZnSe within the local density approximation and have begun the calculation of the gradient correction to these energies. Based on these preliminary numbers, we predict the zinc vacancy and the zinc antisite, and the zinc interstitial to be the dominant defects in ZnSe. We are currently calculating the relaxation about the most important defects in ZnSe.

CONTENTS

1. NATIVE POINT DEFECTS IN IRFPA ACTIVE AND SUBSTRATE MATERIALS 1
   - 1.1 Native Point Defects 1
   - 1.2 Dislocation Strain Fields and Piezoelectric Potentials 1
   - 1.3 Dislocation Core Charges 2
2. PHOTONIC MATERIALS 5
   - 2.1 Wide-Gap II-VI Compounds (ZnSe as Prototype) 5
   - 2.2 Nonlinear Optical Materials ($LiNbO_3$ as Prototype) 6
3. WORK PLANNED 7

REFERENCES 7

APPENDIX

Piezoelectric Potential at a 60° Dislocation in Sphalerite 8

1. NATIVE POINT DEFECTS IN IRFPA ACTIVE AND SUBSTRATE MATERIALS

1.1 NATIVE POINT DEFECTS

In the first quarter, we reported the results of native defect concentrations in $Hg_{0.8}Cd_{0.2}Te$. During the second quarter, we have focused on refining the defect formation energies used in those predictions. In particular, we have begun the calculation of the relaxation energies about the native defects in HgCdTe. We are focusing on the important defects in $Hg_{0.8}Cd_{0.2}Te$, and the mercury interstitial, which is important to mercury diffusion and for which strain energies are expected to be large.

Our original scheme to calculate the relaxations using the Harris approximation, in which the position of the relaxed atoms is calculated non-self-consistently, has proved to be inadequate for cases in which the relaxations are large. Thus, the position of the relaxed atoms must be found self-consistently. We are currently completing these self-consistent calculations for the mercury vacancy, the tellurium antisite, and the mercury interstitial. We expect these calculations to be completed in the next quarter and improved predictions of defect concentrations to be made at that point. The relaxation calculations are also being extended to larger supercells. These calculations are computationally time-consuming, and availability of supercomputer time would expedite our work.

1.2 DISLOCATION STRAIN FIELDS AND PIEZOELECTRIC POTENTIALS

We pointed out in Quarterly Technical Report 1 that the MCT crystal structure lacks inversion symmetry and therefore is piezoelectric, and that the strain-induced bound charge density and the fields that it generates can affect the transport properties of the semiconductor. We reported on a first approach to this issue, and we have continued the work in the current quarter.

The strain field around a dislocation can generate an electric field, and conversely an electric field applied to a piezoelectric crystal can produce a stress that may deform the crystal. This self-consistent field problem has been treated rigorously for a straight dislocation in a homogeneous insulating crystal (intrinsic wide-gap semiconductor) by Saada (1971). The general analysis was extended by Faivre and Saada (1972) to include the effects of screening by free carriers. Several qualitatively significant conclusions can be drawn from this work: (1) The strains are only slightly affected by the electric field; that is to say, the inverse piezoelectric effect is small, and the electric field can be calculated directly without imposing the requirement of self-consistency. (2) The electric field in the vicinity of the dislocation core can be quite large, and the dislocation can interact strongly with charges (point defects or mobile carriers) in

its vicinity. (3) In a semiconductor the dislocation preferentially traps carriers of a particular sign. (4) The estimated screening distance is of the order of several Debye lengths.

Booyens and Vermaak (1979) have applied Saada's analysis to ⟨110⟩ dislocations in zincblende III-V semiconductors, and Booyens and Basson (1984) to CdTe and MCT. They do not explicitly include the effects of screening as analyzed by Faivre and Saada (1972) in these calculations. As a result, they find that an uncharged dislocation, in the absence of screening, generates a net radial field. They suggest that the dislocation core is likely to acquire a charge that compensates for the radial field and so minimizes the total energy of the dislocation. While this is a plausible suggestion, it does depend on unknown details of the core electronic states and needs to be examined more closely. We have similarly extended the analysis to the commonly observed 60° dislocations in intrinsic MCT and obtained detailed plots of the electric potential distribution arising from the strain about a straight dislocation. We find that the potential is a superposition of cylindrical quadrupole and hexadecapole terms. The theory and initial results of the calculation are given in the Appendix. These results are preliminary, since they do not yet take into account screening by free carriers, anisotropy, and interactions among a distribution of dislocations.

1.3 DISLOCATION CORE CHARGES

The fields associated with electrically charged dislocation cores can act as scattering and recombination centers and may attract or repel charged point defects. As pointed out above in connection with the strain-induced charges and fields, the presence and amount of charge on a dislocation core depend on the distribution of gap levels in the core and on the Fermi level in the semiconductor. Here we take a phenomenological view and consider the electric field and potential generated by a given core charge, determined from the band bending around an inverted core. The band gap of the material sets the boundary condition for the potential at the core radius. We assume, conservatively, a core radius of 5 Å and a core edge potential of 0.1 eV, equal to the band gap. The effective radius of the field is taken to be that distance from the dislocation core within which the field is large enough to move a carrier the distance between dislocations in a minority carrier lifetime (as measured in dislocation-free material). The rationale for this assumption is that a field smaller than this is not likely to affect the carrier lifetime or mobility. If we use a lifetime of 10^{-6} s and a mobility of 10^5 cm^2/Vs, this sets the minimum effective field at approximately $10n_D^{-1/2}$ V/cm, with the dislocation density n_D in cm^{-2}. This is used to determine a numerical threshold field.

The principle of the calculation, both in the depletion approximation and with screening, was given in Appendix B of Quarterly Report 1. We have now extended the work, using a better value of the optical range dielectric constant (Brice and Capper 1987), and taking into account the temperature dependence of the Debye frequency.

The results are summarized in Figure 1. The figure shows two sets of results: the radius R of the field region surrounding the positively charged core as a function of carrier density calculated on the basis of the depletion approximation, and the screening radius l of the region inside which the electric field due to the charged core exceeds 10 mV. This threshold for the

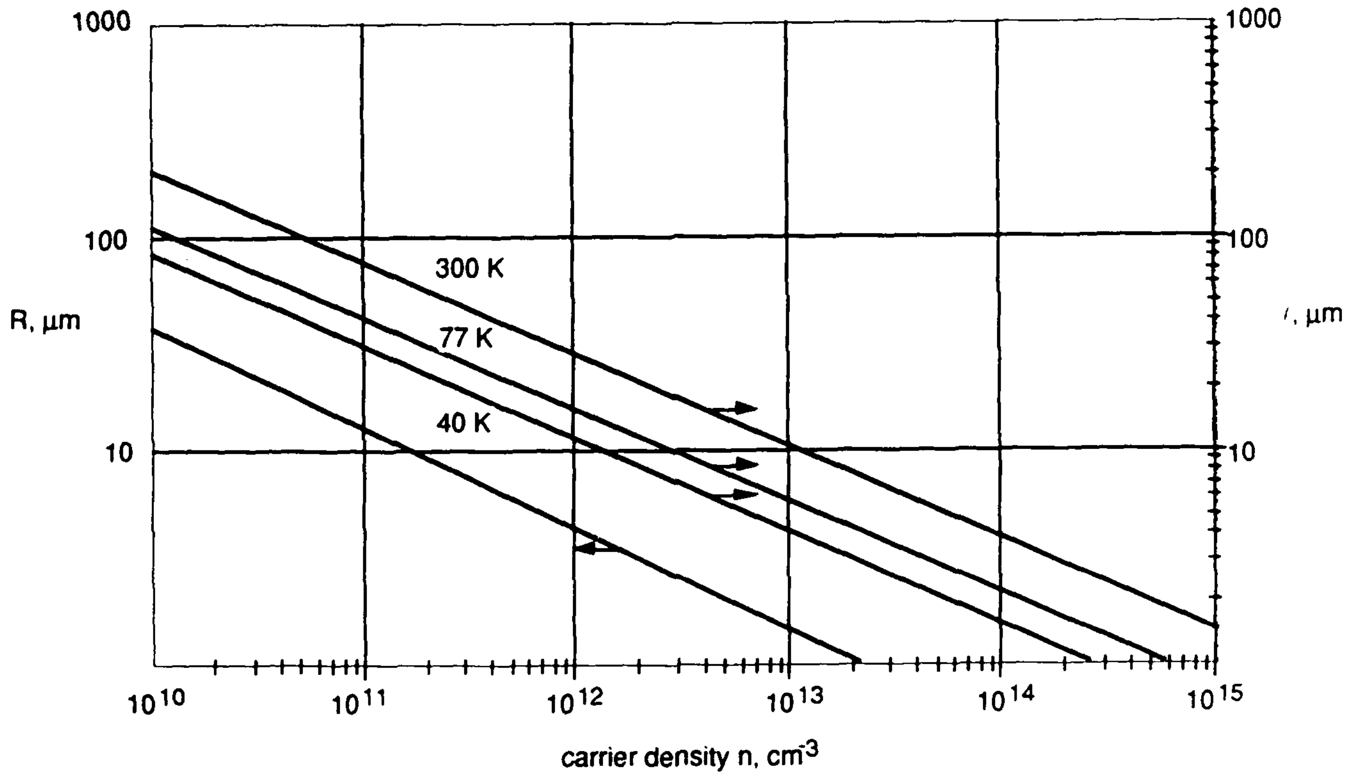

Figure 1. Dependence of space charge radius R (depletion approximation) and screening radius ℓ on carrier density. For the range shown here, we find $\ell \propto n^{-0.43}$.

be-120893-sd

electric field is based on the experimental observations of Johnson et al. (1992) and Shin et al. (1992) that the R_0A values and minority carrier lifetimes decrease rapidly with the dislocation density n_D when it exceeds 10^6 cm^{-2}. The calculation of the screening radius ℓ is more reliable than the depletion approximation, since it takes into account the thermal agitation of the carriers. With the parameters we use, the calculation of the screening radius over five orders of magnitude of the carrier density, and over the temperature range of 40 to 300 K, results in values of ℓ that range from about 5 L_D (Debye lengths) at $n = 10^{10}$ cm^{-3} to 10 L_D at $n = 10^{15}$ cm^{-3}, resulting in an overall decrease of ℓ with carrier density at a rate slightly slower than $L_D^{-1/2}$.

The carrier density in the neutral region of the extrinsic device material generally equals or exceeds 10^{14} cm^{-3}. The screening length at this carrier density even at room temperature is less than 4 µm, and only about 1.5 µm at 40 K. Since the mobile carrier density in the neutral regions generally exceeds 10^{14} cm^{-3}, we can conclude that in the presence of mobile carriers, especially at cryogenic temperatures, the core charge fields have a limited range, in rough agreement with the observed small variation of the responsivity with dislocation density.

The situation is less clear in an extended depletion region, such as the vicinity of the metallurgical junction of the detector. In this region the carrier density is reduced to the intrinsic value n_i under zero bias, and below this with a reverse bias. We estimate a value of n_i of about 5×10^{11} cm^{-3} for $Hg_{0.8}Cd_{0.2}Te$ at 40 K, with a decrease of approximately a factor of 2 for every 5 mV of reverse bias caused by the separation of the quasi Fermi levels. This reduction of the carrier density is confined to a small region, and an assessment of its quantitative effect will require detailed computation. Nonetheless, it is worth observing that for this carrier density we estimate a screening radius of 17 μm, consistent with the experimental finding (Johnson et al., 1992) that R_0A at this temperature is already decreasing with dislocation density in this range. The literature values of $n_i = 1.2 \times 10^{14}$ cm^{-3} at 77 K and $n_i = 4.0 \times 10^{16}$ cm^{-3} at 300 K (quoted in Brice and Capper, 1987) correspond to progressively shorter screening lengths, which is also consistent with the experimental observation that the decrease in R_0A with dislocation density has a higher threshold at the higher temperature.

Thus, to summarize we find that dislocations impact device performance through two possible mechanisms: core line charge accompanied by a depletion layer with radial field surrounding it, and an angular potential variation arising from the long-range strain and the piezoelectric effect. In a neutral region of the semiconductor—that is, the n-region below the depletion layer in a p-on-n heterojunction diode—screening prevents the dislocations from greatly influencing device characteristics. As a consequence, the responsivity of such devices, which is dominated by the minority carrier recombination lifetime, varies slowly with dislocation density. However, in the depletion region screening is greatly reduced, and the long-range angular potential produced by a dislocation that threads through the depletion region is capable, in principle, of increasing the tunneling currents at low temperature as observed. We need an accurate value for the HgCdTe piezoelectric coefficient and a determination of the core charge states of the various dislocation types before we can, with more assurance, specify the mechanism through which dislocations affect the responsivity and noise of devices. Some dislocation types are certain to be more troublesome than others in a given device structure. Once the worst offenders are identified we can begin to design ways to eliminate or passivate them.

2. PHOTONIC MATERIALS

2.1 WIDE-GAP II-VI COMPOUNDS (ZnSe AS PROTOTYPE)

We have completed the local density calculation of the formation energies for the neutral unrelaxed native defects in ZnSe. The defects we have considered are the cation and anion vacancies V_{Zn} and V_{Se}, the cation and anion antisite Se_{Zn} and Zn_{Se} and the cation and anion interstitial Se_I and Zn_I. The interstitial site considered is tetrahedral, where the four first neighbors are cations; we will later return to calculation for the tetrahedral site where the four first neighbors are anions. The defect reactions considered are

$$ZnSe \rightarrow V_{Zn}Se + Zn_g \quad (1)$$

$$Zn_g \rightarrow Zn\ V_{Se} \quad (2)$$

$$2Zn_g \rightarrow Zn\ Zn_{Se} \quad (3)$$

$$2ZnSe \rightarrow Se_{Zn}Se + 2Zn_g \quad (4)$$

$$Zn_g \rightarrow Zn_I \quad (5)$$

$$ZnSe \rightarrow Se_I + Zn_g \quad (6)$$

where Zn_g is the zinc in the free atom state.

The calculation of the defect formation energies consists of several steps. First, the formation energy from the unrelaxed lattice is calculated. These energies for the 16-atom supercell are given in Table 1. To these energies the gradient correction to the local density formation energies must be added. This correction is important when the free atom is used as a reference state, as is the case when we wish to consider the vapor pressure as an external free variable. The gradient corrections for the defects have been completed using a coarse mesh for the k-space Brillouin zone integration. Based on these calculations, the gradient corrections for defect reactions 1 through 6 are sizable, ranging from 0.2 to 0.8 eV, and thus merit a more precise calculation. The self-consistent charge densities from the coarse mesh calculation are being used to calculate the gradient correction self-consistently on a finer mesh. These calculations are nearly done and will be reported in the next quarter.

The relaxation energy must be calculated by allowing the overall lattice constant to obtain a minimum, and searching for the minimum energy position of the near-neighbor atoms. The former relaxation has been completed, and this relaxation energy is included in the energies given in Table 1.

Table 1

DEFECT FORMATION ENERGIES AND ENTROPIES FOR THE NEUTRAL, UNRELAXED DEFECTS. Energies do not include the gradient correction

Defect	Energy (eV)	Entropy (k_B)
V_{Zn}	5.00	−7.58
VSe	0.76	8.34
Zn_{Se}	−1.23	15.9
Se_{Zn}	9.40	−16.0
Zn_I	1.08	7.91
Se_I	7.37	−7.91

We are currently calculating the second contribution to the relaxation energy. We have been experimenting with non-self-consistent schemes whereby the charge densities about each atom, for example in the unrelaxed configuration, are used to calculate the energy for the lattice in a relaxed configuration using a Harris approach. While this method appears to be reliable for small distortions, it appears to be unreliable for the large distortions we are finding about the interstitial and antisite defects. Thus, we are forced to complete self-consistent calculations of the relaxation, which entail a large amount of computer time. Because our rate of progress is limited by the speed of our in-house computer, which is timeshared among several projects, availability of supercomputer resources from DARPA would expedite these calculations. Our codes have previously been optimized for operation on many machines, including the CRAY series.

Temperature-dependent defect formation entropies have been calculated. These entropies are a necessary ingredient in the calculation of the native defect densities. When a defect is created in the ZnSe lattice, the phonon modes of the crystal are modified, and these modifications contribute to the defect formation entropy. To calculate this contribution to the defect formation entropy, we have used a valence force-field model for the lattice phonons. A Green's function method is then used to introduce a localized perturbation, for example a vacancy or an antisite, into the lattice. From the change in the density of (vibrational) states, the defect formation entropy can be calculated. The formation entropies in units of Boltzmann's constant for 800 °C are given in Table 1. These entropies correspond to the reactions in Eqs. 1 through 6 above.

2.2 NONLINEAR OPTICAL MATERIALS ($LiNbO_3$ AS PROTOTYPE)

The work on $LiNbO_3$ is scheduled to start in the next quarter.

3. WORK PLANNED

During the next quarter, we expect to complete the calculation of the relaxation of the near neighbors about the most important native defects in both HgCdTe and ZnSe, and to complete the gradient correction to the defect energies in ZnSe. We expect to make preliminary estimates of native defect densities in ZnSe, and to refine those in HgCdTe. Work will commence on the properties of $LiNbO_3$.

REFERENCES

Booyens, H., and J.H. Basson, 1984. "Piezoelectrically induced charge distributions around dislocations in CdTe and HgCdTe," *Phys. Stat. Sol.* (a) 85, 243.

Booyens, H., and J.S. Vermaak, 1978. "Piezoelectric coupling and dislocations in III-V compounds," *J. Appl. Phys.* 50, 4302.

Brice, J., and P. Capper, eds., 1987. *The properties of mercury cadmium telluride,* EMIS Data Reviews, Series No. 3, INSPEC, New York.

Faivre, G., and G. Saada, 1972. "Dislocations in piezoelectric semiconductors," *Phys. Stat. Sol.* (b) 52, 127.

Johnson, S.N., D.R. Rhiger, J.P. Rosbeck, J.M. Peterson, S.M. Taylor, and M.E. Boyd, 1992. "Effects of dislocations on the electrical and optical properties of long-wavelength infrared HgCdTe photovoltaic detectors," *J. Vac. Sci. Technol.* B 10, 1499.

Saada, G., 1971 "Dislocations dans les cristaux piézoélectriques," *Phys. Stat. Sol.* (b) 44, 717.

Shin, S.H., J.M. Arias, D.D. Edwall, M. Zandian, J.G. Pasko, and R.E. DeWamas, 1992. "Dislocation reduction in HgCdTe on GaAs and Si," *J. Vac. Sci. Technol.* B 10, 1492.

Appendix

PIEZOELECTRIC POTENTIAL AT A 60° DISLOCATION IN SPHALERITE

The dislocation lies along $[\bar{1}01]$ and has a Burgers vector **b** at 60° to the dislocation line ξ. The edge component of the Burgers vector b^e is chosen as x_1. x_2 is the normal to the slip plane, and x_3 is ξ (Figure A-1). The transformation matrix from principal axis coordinates is

$$T_{ij} = \frac{1}{\sqrt{6}}\begin{pmatrix} 1 & -2 & 1 \\ \sqrt{2} & \sqrt{2} & \sqrt{2} \\ -\sqrt{3} & 0 & \sqrt{3} \end{pmatrix}.$$

The transformation of the piezoelectric tensor is

$$d'_{ijk} = T_{ip}T_{jq}T_{kr}d_{pqr}.$$

In cubic symmetry and principal axis coordinates all the nonzero components of the piezoelectric tensor are equal $d_{123}=d_{132}=d_{231}=d_{213}=d_{312}=d_{321}=d$.

The nonzero components of the transformed tensor (d') are

$$\begin{aligned} &d'_{133} = d'_{313} = d'_{331} = -d'_{111} = \frac{2}{\sqrt{6}}d \\ &d'_{112} = d'_{121} = d'_{211} = d'_{233} = d'_{323} = d'_{332} = -\frac{1}{\sqrt{3}}d \\ &d'_{222} = \frac{2}{\sqrt{3}}d\,; \end{aligned} \tag{1}$$

in two-index (Voigt) notation

$$(d') = \begin{pmatrix} -\frac{2}{\sqrt{6}}d & 0 & \frac{2}{\sqrt{6}}d & 0 & 0 & -\frac{1}{\sqrt{3}}d \\ -\frac{1}{\sqrt{3}}d & \frac{2}{\sqrt{3}}d & -\frac{1}{\sqrt{3}}d & 0 & 0 & 0 \\ 0 & 0 & 0 & -\frac{1}{\sqrt{3}}d & \frac{2}{\sqrt{6}}d & 0 \end{pmatrix}.$$

The piezoelectrically induced bound charge density is

$$\rho(\mathbf{r}) = \frac{1}{\varepsilon}d_{ijk}e_{jk,i} \quad \text{with } e_{jk,i} \equiv \frac{\partial}{\partial x_i}e_{jk} \tag{2}$$

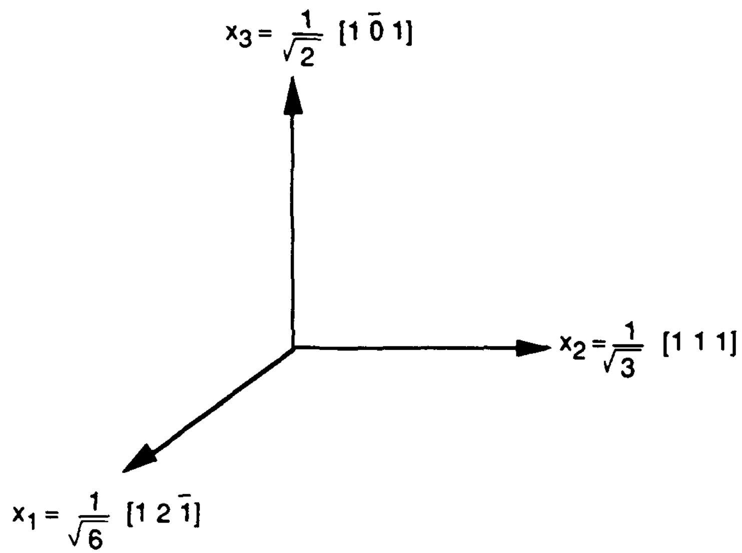

(a) Definition of coordinate system

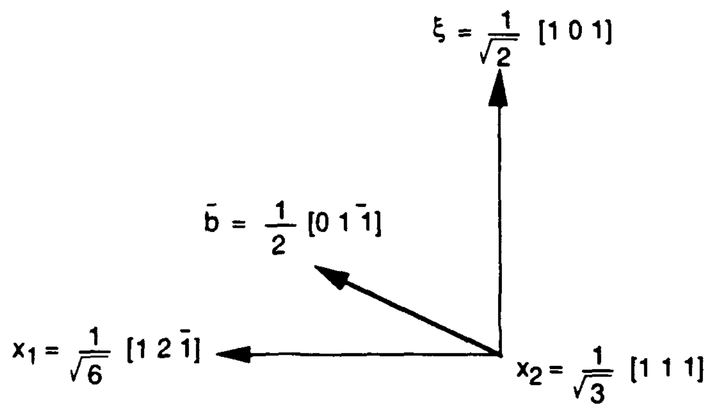

(b) Orientation of line vector $\bar{\xi}$ and Burgers vector $\bar{b}$ of a 60° dislocation

Figure A-1. Geometry used in calculating properties of dislocations

bc-220893-sd

where ε is the isotropic dielectric constant, e_{jk} is the jk component of the strain tensor, and summation over repeated indexes is implied.

For a screw dislocation in linear anisotropic theory the displacements are

$$u_3 = -\frac{b_3}{2\pi}\tan^{-1}A\left(\frac{x_2}{x_1}\right), u_1 = u_2 = 0 ,$$

where

$$A = \frac{\sqrt{c'_{44}c'_{55}}}{c'_{44}};\ c'_{44} = c_{44} - \frac{1}{3}H;\ c'_{55} = c_{44} - \frac{1}{6}H;\ H = 2c_{44} + c_{12} - c_{11} .$$

Here, c_{ij} and c'_{ij} are the components of the elastic tensor in the principal axis and transformed coordinate systems, respectively. The nonzero components of the strain tensor are, using

$$e_{ij} = \frac{1}{2}\ (u_{i,j} + u_{j,i}):\ e_{13} = e_{31} \text{ and } e_{23} = e_{32}; \text{ all others zero.}$$

Using (1) and (2) shows immediately that for this case $\rho = 0$.

For an edge dislocation, with ν Poisson's ratio

$$u_1 = \frac{b}{2\pi}\left[\tan^{-1}\left(\frac{x_2}{x_1}\right) + \frac{x_1x_2}{2(1-\nu)(x_1^2+x_2^2)}\right];$$

$$u_2 = -\frac{b}{2\pi}\left[\frac{1-2\nu}{4(1-\nu)}\ln(x_1^2+x_2^2) + \frac{x_1^2-x_2^2}{4(1-\nu)(x_1^2+x_2^2)}\right];$$

$$u_3 = 0.$$

The nonzero strain components are

$$e_{11} = \frac{b}{2\pi}\frac{(1-2\nu)x_2^3+(3-2\nu)x_1^2x_2}{2(\nu-1)(x_1^2+x_2^2)^2}$$

$$e_{22} = \frac{b}{2\pi}\frac{(1-2\nu)x_2^3-(1+2\nu)x_1^2x_2}{2(\nu-1)(x_1^2+x_2^2)^2}$$

$$e_{12} = \frac{b}{2\pi}\frac{x_1x_2^2-x_1^3}{2(\nu-1)(x_1^2+x_2^2)^2} .$$

From (2) and (1)

$$\rho(r) = \frac{1}{\varepsilon}\left(d'_{111}e_{11,1} + 2d'_{112}e_{12,1} + d'_{211}e_{11,2} + d'_{222}e_{22,2}\right)$$

so we need the derivatives

$$e_{11,1} = \frac{b}{2\pi}\frac{(2\nu+1)x_1x_2^3+(2\nu-3)x_1^3x_2}{(\nu-1)(x_1^2+x_2^2)^3}$$

$$e_{11,2} = \frac{b}{2\pi}\frac{(2\nu-1)x_2^4-6x_1^2x_2^2+(3-2\nu)x_1^4}{2(\nu-1)(x_1^2+x_2^2)^3}$$

$$e_{22,2} = \frac{b}{2\pi}\frac{(2\nu-1)x_2^4+6x_1^2x_2^2-(2\nu+1)x_1^4}{2(\nu-1)(x_1^2+x_2^2)^3}$$

$$e_{12,1} = \frac{b}{2\pi}\frac{x_2^4-6x_1^2x_2^2+x_1^4}{2(\nu-1)(x_1^2+x^2)^3}$$

giving

$$\rho(x_1, x_2) = \frac{d}{\sqrt{3}\varepsilon}\left(-\sqrt{2}\,e_{11,1} - 2e_{12,1} - e_{11,2} + 2e_{22,2}\right)$$

$$= \frac{bd}{2\pi\sqrt{3}\varepsilon}\;\frac{(2\nu-3)x_2^4-2\sqrt{2}(2\nu+1)x_1x_2^3+30x_1^2x_2^2+2\sqrt{2}(3-2\nu)x_1^3x_2-(2\nu+7)x_1^4}{2(\nu-1)\left(x_1^2+x_2^2\right)^3}\;.$$

When this expression is converted to polar coordinates in the x_1x_2 plane (xyplane) this becomes a somewhat simpler expression that has a radial r^{-2} dependence with angular terms having quadrupole and hexadecapole form:

$$\rho = \frac{bd}{2\pi\sqrt{3}\varepsilon}\;(\rho_1 + \rho_2 + \rho_3 + \rho_4 + \rho_5)$$

with

$$\rho_1 = \frac{(2\nu-3)}{2(\nu-1)}\frac{y^4}{r^6} = \frac{(2\nu-3)}{2(\nu-1)}\frac{\cos4\theta-4\cos2\theta+3}{8r^2}$$

$$\rho_2 = \frac{-2\sqrt{2}(2\nu+1)}{2(\nu-1)}\frac{xy^3}{r^6} = \frac{-2\sqrt{2}(2\nu+1)}{2(\nu-1)}\frac{2\sin2\theta-\sin4\theta}{8r^2}$$

$$\rho_3 = \frac{30}{2(\nu-1)}\frac{x^2y^2}{r^6} = \frac{30}{2(\nu-1)}\frac{1-\cos4\theta}{8r^2}$$

$$\rho_4 = \frac{2\sqrt{2}(3-2\nu)}{2(1-\nu)}\frac{x^3y}{r^6} = \frac{2\sqrt{2}(3-2\nu)}{2(\nu-1)}\frac{\sin4\theta+2\sin2\theta}{8r^2}$$

$$\rho_5 = \frac{-(2\nu+7)}{2(\nu-1)}\frac{x^4}{r^6} = \frac{-(2\nu+7)}{2(\nu-1)}\frac{\cos4\theta+4\cos2\theta+3}{8r^2}$$

so

$$\rho = \frac{bd}{4\pi\sqrt{3}\varepsilon(1-\nu)}\frac{1}{r^2}[5\cos4\theta-\sqrt{2}\sin4\theta+2(1+\nu)\cos2\theta-\sqrt{2}(1-\nu)\sin2\theta]$$

$$= \frac{C}{r^2}\sum_{n=2,4}[a_n\cos(n\theta)+b_n\sin(n\theta)$$

To obtain the piezoelectric potential we need to solve the Poisson equation

$$\nabla^2\Phi = -\frac{4\pi\rho}{\varepsilon}$$

with this charge distribution as the source. In two dimensions the formal solution of the Poisson equation is

$$\Phi(r,\theta) = \frac{1}{\pi}\int_0^\infty r'dr'\int_0^{2\pi} d\theta'\left[\ln\frac{1}{r_>} + \sum_{m=1}^{\infty}\frac{1}{m}\left(\frac{r_<}{r_>}\right)^m \cos m(\theta-\theta')\right]\rho(r')$$

$$= \frac{C}{\pi}\sum_{m=1}^{\infty}\frac{1}{m}\int_0^{2\pi} d\theta'[\sin(m\theta)\sin(m\theta')+\cos(m\theta)\cos(m\theta')]\times$$

$$\times\sum_{n=2,4}[a_n\cos(n\theta')+b_n\sin(n\theta')]\int_0^\infty\frac{r'dr'}{r'^2}\left(\frac{r_<}{r_>}\right)^m$$

where $r_>$ and $r_<$ are the greater and lesser, respectively, of r and r'.

The integral diverges at the origin because of the r^{-2} dependence of ρ. To deal with this difficulty we adopt the same procedure that is used to avoid the divergence of the elastic energy of a dislocation at the origin in continuum theory. We set cutoffs at an inner radius R_1 and an outer radius R_2. The cutoff at R_1 removes the core singularity, and the cutoff at R_2 allows ρ to be expanded in multipoles. Later we will identify R_1 as the core radius and we will let $R_2 \rightarrow \infty$. We now have

$$\Phi(r,\theta) = \frac{C}{\pi} \sum_{n=2,4} \frac{\pi}{n} \left[a_n\cos(n\theta)+b_n\sin(n\theta) \left(\frac{1}{r^n} \int_{R_1}^{r} (r')^{n-1} dr' + r^n \int_{r}^{R_2} (r')^{-n-1} dr' \right) \right.$$

$$= C\left\{ \frac{1}{4} [a_4\cos(4\theta)+b_4\sin(4\theta)] \left[\frac{1}{2} - \frac{1}{4}\left(\frac{R_1}{r}\right)^4 - \frac{1}{4}\left(\frac{r}{R_2}\right)^4 \right] \right.$$

$$\left. + \frac{1}{2} [a_2\cos(2\theta)+b_2\sin(2\theta)] \left[1 - \frac{1}{2}\left(\frac{R_1}{r}\right)^2 - \frac{1}{2}\left(\frac{r}{R_2}\right)^2 \right] \right\}$$

for $r < R_2$. For $r > R_2$

$$\Phi(r,\theta) = C\left\{ \frac{1}{4} [a_4\cos(4\theta)+b_4\sin(4\theta)] \frac{1}{4}\left[\left(\frac{R_2}{r}\right)^4 - \left(\frac{R_1}{r}\right)^4 \right] \right.$$

$$\left. + \frac{1}{2} [a_2\cos(2\theta)+b_2\sin(2\theta)] \frac{1}{2}\left[\left(\frac{R_2}{r}\right)^2 - \left(\frac{R_1}{r}\right)^2 \right] \right\}$$

which is a multipole potential. The two solutions are matched at R_2. We can now let $R_2 \rightarrow \infty$ and neglect the terms in R_1, which amount to a small correction near the core, to get a potential valid for $r >> R_1$

$$\Phi(r,\theta) = C\left\{ \frac{1}{8} [a_4\cos(4\theta)+b_4\sin(4\theta)] + \frac{1}{2} [a_2\cos(2\theta)+b_2\sin(2\theta)] \right\}$$

which is independent of r.

For numerical calculation we would need the piezoelectric constant of the alloy, which has not been determined. To get an order of magnitude estimate, we can use the piezoelectric constant of CdTe, 3×10^{-6} C cm^{-2}. The Burgers vector is 4×10^{-8} cm, and Poisson's ratio can be taken as 0.3. Using these values we have computed the charge, potential, and field plots of Figure A-2.

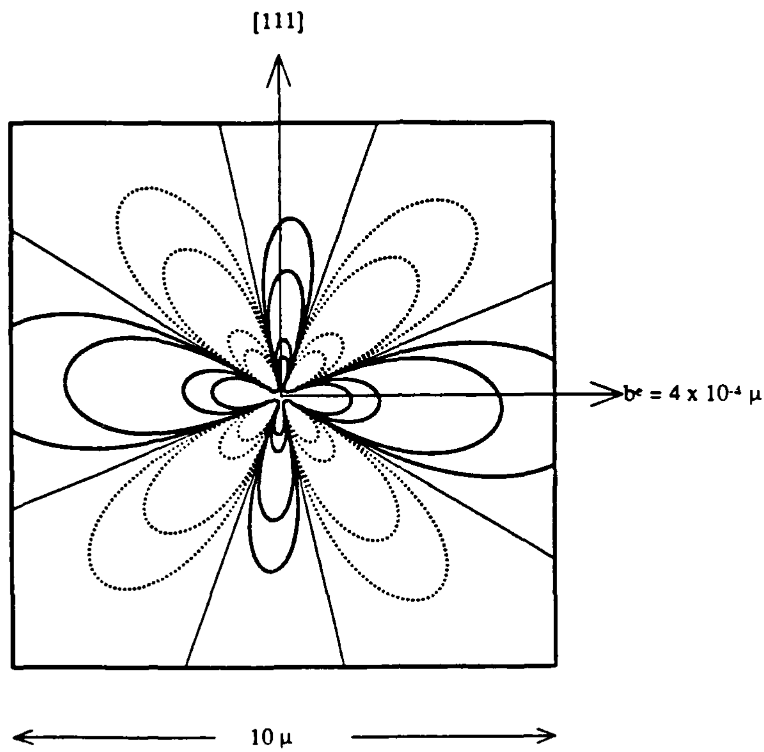

(a) Piezoelectric charge normal to the dislocation line. Solid contours are 1, 0.5 0.1, and 0.05 10^{12} e/cm^3 going out radially; dotted contours are the negative of these.

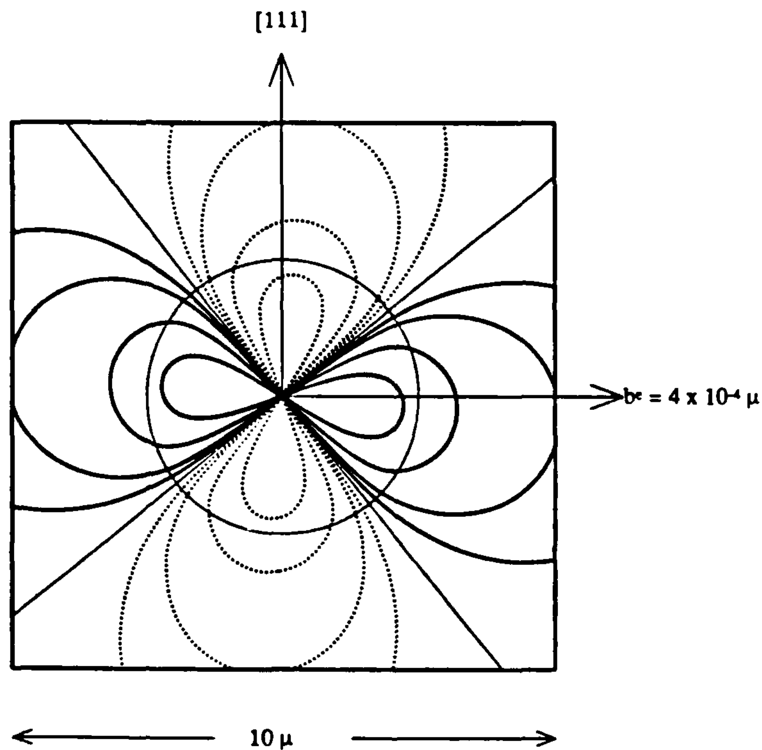

(b) Quadrupole component of the piezoelectric potential.

Figure D-2. Piezoelectric properties of a 60° dislocation in $Hg_{0.8}Cd_{0.2}Te$

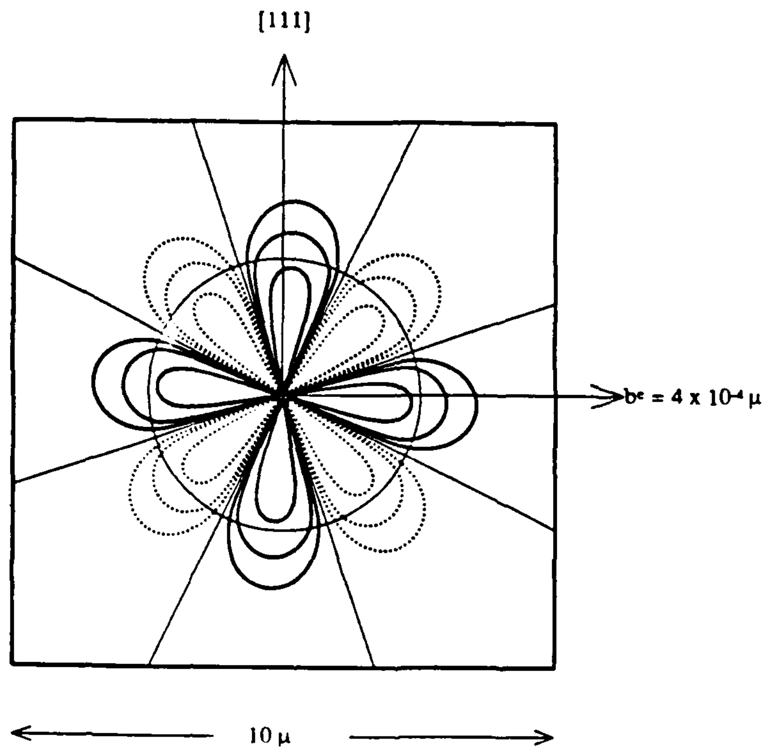

(c) Hexadecapole component of the piezoelectric potential

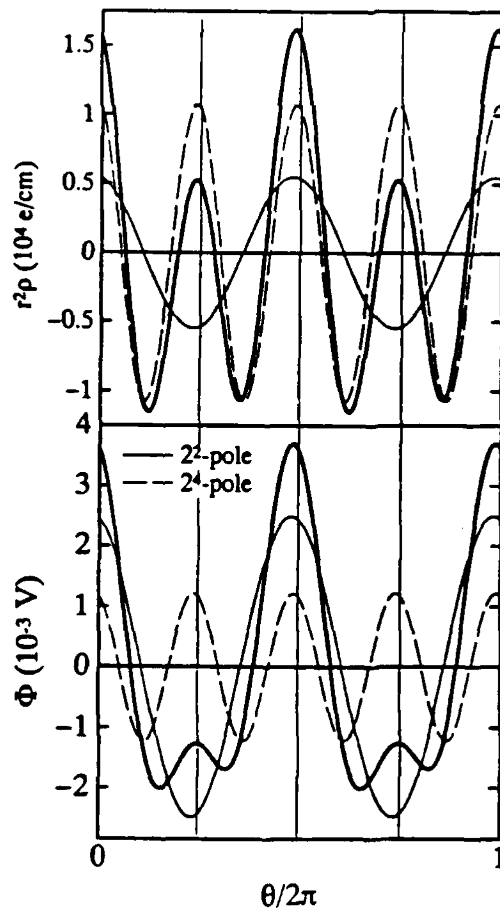

(d) Angular variation of the piezoelectric charge and potential normal to the dislocation line

Figure D-2. Continued